PROGRESS IN COLOR, COLORANTS AND COATINGS

available online @ www.pccc.icrc.ac.ir

Progress in Color Colorants Coating 19 (2026), 9-22

Ministry of Science, Research and Technology
Institute for Color Science & Technology

Corrosion Protection of Mild Steel in Acidic Media by a Triazole-Based Inhibitor: Mechanistic Insights and Performance Evaluation

N. A. Al-Ali[1], A. Alamiery[*2]

[1.] Biomedical Engineering Department, University of Technology, Baghdad P.O. Box: 10001, Baghdad, Iraq

[2.] Biomedical Engineering Department, College of Engineering, Al-Ayen University (AUIQ), Nile St, Nasiriyah P.O. Box: 64001, Dhi Qar, Iraq

ARTICLE INFO

Article history:
Received: 20 Apr 2025
Final Revised: 20 Jun 2025
Accepted: 23 Jun 2025
Available online: 22 Sep 2025

Keywords:
Corrosion inhibition
Weight loss method
DFT
Temperature effect on corrosion

ABSTRACT

The present work investigates the corrosion inhibition behavior of 4-(4-methoxybenzylidene)amino-5-pyridin-3-yl-3-thio-1,2,4-triazole (MAPTT) on mild steel in 1 M HCl using the weight loss method over a range of concentrations (0.1-1.0 mM) and immersion durations (1-48 hours). The inhibition efficiency (IE%) was found to rise with increasing inhibitor concentration, achieving a maximum value of 92.7% at 0.5 mM after 48 hours. Although a gradual improvement in efficiency was observed with longer immersion periods, it tended to stabilize after 10 hours. Investigations at different temperatures (303–333 K) over a 5-hour immersion period revealed a slight improvement in inhibition efficiency, suggesting good thermal stability of MAPTT. The process of adsorption obeyed Langmuir model, referring to a combination of chemical and physical adsorption mechanisms. In comparison with previously reported inhibitors, MAPTT demonstrated superior performance, attributed to its strong adsorption and stable protective film formation at elevated temperatures, ensuring sustained corrosion resistance. Density Functional Theory (DFT) predictions, having the analysis of HOMO and LUMO orbitals, identified active adsorption centers within the molecule. Furthermore, the calculated band gap in addition to electron transfer fraction (ΔN) supported the strong interactions between MAPTT and specimen surface. The excellent correlation of experimental techniques and theoretical DFT calculations highlights the promise of MAPTT as a thermally robust and highly efficient corrosion inhibitor for industrial use in corrosive solution. Prog. Color Colorants Coat. 19 (2026), 9-22© Institute for Color Science and Technology.

1. Introduction

All industries face and suffer from the critical problem of corrosion, especially in environments involving acidic media [1, 2]. Mild steel is widely utilized across numerous industries due to its cost-effectiveness and favorable mechanical properties; however, it is highly susceptible to corrosion in acidic environments, resulting in significant economic losses and safety concerns in industrial operations [3]. In this study, 1 M HCl was chosen as the corrosive medium to evaluate the performance of MAPTT, as it is a widely used acidic solution in various industrial processes such as acid pickling, industrial descaling, boiler cleaning, and petroleum refining [4]. These processes expose metal equipment to highly aggressive environments, necessi-tating the use of effective corrosion inhibitors.

*Corresponding author: * dr.ahmed1975@gukm.edu.my
dr.ahmed1975@gmail.com

https://doi.org/ 10.30509/pccc.2025.167535.1392

Conventional corrosion prevention methodologies often include toxic and environmentally unfriendly inhibitors [5, 6]. Hence, it is very necessity to develop and find out effective environmentally friendly inhibitors. The most effective technique to mitigate corrosion is the employment of inhibitors, which adsorb onto tested specimens and form a protective barrier [7, 8]. From different types of the inhibitors, the one with heteroatoms such as nitrogen, sulfur, and oxygen namely organic compounds, have garnered significant attention due to their superior inhibition efficiencies and eco-friendly nature [9-12]. Recent studies have concentrated on designing and optimizing corrosion inhibitors that incorporate heteroatoms. These heteroatoms enhance adsorption on metal surfaces through chemisorption and physisorption mechanisms. For instance, a study published by Abuelela, et al. highlighted that organic compounds containing these heteroatoms exhibit significant efficacy due to ability to be adsorbed onto specimen surface, thereby reducing corrosion rates [13]. Additionally, there is a growing interest in Schiff bases, triazole derivatives, and hybrid organic-inorganic compounds for their superior corrosion resistance in acidic environments. A 2023 study by Gad et al. investigated the performances of Schiff base in inhibition the mild steel corrosion in acidic media, demonstrating their potential as efficient corrosion inhibitors [14, 15]. Likewise, triazole-based compounds have demonstrated strong adsorption capabilities on the metal, particularly under aggressive conditions, owing to their polar functional groups and their tendency to form stable complexes with metal atoms [16, 17]. Although triazole-based compounds have been widely investigated for their corrosion inhibition potential, studies specifically focusing on the performance of 4-(4-methoxybenzylidene)amino-5-pyridin-3-yl-3-thio-1,2,4-triazole (MAPTT) remain scarce. As shown in Figure 1, MAPTT contains several structural moieties that are known to enhance adsorption on metal surfaces: a triazole ring, which provides multiple coordination sites; a thio group (-C=S) and a pyridine ring, which contain electronegative nitrogen and sulfur atoms; and a methoxy-substituted benzylidene fragment, which contributes π-electron density for additional surface interaction. The combination of these functional groups facilitates both chemisorption (via lone pair donation and π–d orbital overlap) and physisorption (through electrostatic interactions), potentially offering strong and thermally stable adsorption on steel surfaces.

To address the existing gap in the literature, this study evaluates the corrosion inhibition efficiency of MAPTT for mild steel in 1 M HCl using weight loss techniques across varying concentrations, immersion durations, and temperatures. The adsorption mechanism is analyzed using the Langmuir isotherm model, and to further elucidate the nature of MAPTT–metal interactions, Density Functional Theory (DFT) calculations were performed. These theoretical insights provide a molecular-level understanding of the inhibitor's activity and help establish the relationship between its electronic properties and inhibitory performance.

2. Experimental

2.1. Material and sample preparation

All chemicals and solvents, including hydrochloric acid (HCl) and 4-(4-methoxybenzylidene)amino-5-pyridin-3-yl-3-thio-1,2,4-triazole (MAPTT), were purchased from Sigma-Aldrich (Malaysia and utilized without any further purification. An X-Ray fluorescence (XRF) spectrometer was employed to analyse the chemical composition of the mild steel coupons with the following weight ratios: 0.21 C, 0.05 Mn, 0.09 F, 0.05 S, 0.01 Al, 0.38 Si, and balance Fe. Rectangular specimens measuring 3 × 2 × 0.2 cm were prepared for all experiments. The surface of the specimens was polished sequentially with sandpapers of grit sizes ranging from 360 to 3000 to achieve a smooth and

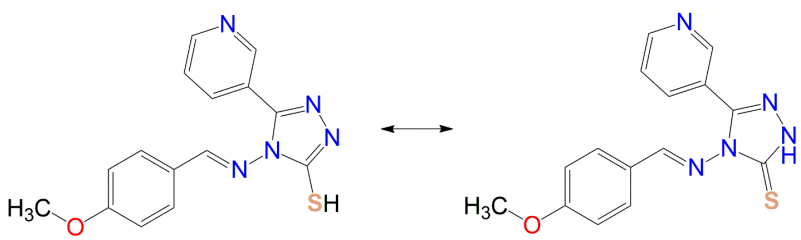

Figure 1: The chemical structure of MAPTT.

uniform finish. After polishing, the specimens were thoroughly washed and cleaned following ASTM G1-03 standard procedures to eliminate any remaining contaminants or surface oxides [18].

2.2. Solution preparation

A stock solution of 1 M HCl was prepared through diluting HCl (37 %) with double distilled water. The corrosion inhibitor, 4-(4-methoxybenzylidene)amino-5-pyridin-3-yl-3-thio-1,2,4-triazole (MAPTT) at varying concentrations (0.1-1 mM), was dissolved in the acidic medium.

2.3. Weight loss method

Weight loss (WL) experiments were performed to assess the corrosion inhibition efficiency of MAPTT, following ASTM G1 standard procedures [18]. The methods were carried out at 303 °K as a controlled temperature, with specimens of tested steel completely immersed in the media which has inhibitor. The initial and final masses of the steel specimens were recorded using a high-precision digital balance after predetermined immersion periods (1, 5, 10, 24, and 48 hours). To evaluate the influence of temperature, additional tests were carried out at 313-333 K, for 5 h, as immersion duration [19]. Weight loss (in milligrams) was indicated by determining the variation between the pre- and post-immersion weights of each sample. To ensure statistical reliability and reproducibility, all measurements were carried out in triplicate.

The inhibition efficiency (IE %) and corrosion rate (C_R, expressed in $gm^{-2}h^{-1}$) were calculated according to equations 1 and 2:

$$IE\% = \frac{W_0 - W_i}{W_0} \times 100 \quad (1)$$

$$C_R = \frac{87.6 \times W}{A \times t \times D} \quad (2)$$

Here, W_o and W_i represent the weight losses of mild steel in 1 M HCl without and with the inhibitor, respectively. W denotes the WL (milligram), A is the area of tested steel which exposed (cm^2), t is the exposed period (hrs), and finally D is the tested steel density.

2.4. Statistical analysis

All weight loss measurements were conducted in triplicate to ensure accuracy and reproducibility. The results are presented as mean values, and standard deviations were calculated to evaluate experimental variability. This statistical approach ensures reliability in interpreting the corrosion rates and inhibition efficiencies. The low variation across replicates confirmed the precision of the experimental method and the stability of MAPTT's inhibitory behavior under the tested conditions.

2.5. Theoretical studies

Calculations of quantum chemical have been carried out and software of Gaussian 09 program was used to investigate the electronic properties of MAPTT [20, 21]. The molecular structure was optimized using the so-called B3LYP function in the basis set 6-31G++(d,p). According to Koopmans' theorem, the calculated ionization potential (I) and electron affinity (A) are directly linked to the energies of the HOMO and LUMO orbitals, as described by equations 3 and 4.

$$E_{HOMO} = -I \quad (3)$$

$$E_{LUMO} = -A \quad (4)$$

Additional molecular parameters, including hardness (η), softness (σ), and electronegativity (χ), were calculated using equations 5 to 7.

$$\eta = \frac{I - A}{2} \quad (5)$$

$$\sigma = \frac{1}{\eta} \quad (6)$$

$$\chi = \frac{I + A}{2} \quad (7)$$

In order to evaluate the charge transfer between the MAPTT and metal, ΔN was determined as follows Eq. 8:

$$\Delta N = \frac{\chi Fe - \chi inhibitor}{2(\eta Fe + \eta inhibitor)} \quad (8)$$

Here, zero absolute hardness (ηFe) is ascribed to bulk iron, whereas the absolute electronegativity was taken as 4.5 eV. The calculations mainly offer the electronic interactions controlling the process of adsorption of MAPTT on mild steel surface, completing the experimental observations.

3. Results and Discussion

3.1. Influence of concentration

Figure 2 illustrates the influence of different MAPTT

concentrations on the C_R and IE % of mild steel immersed in 1 M HCl at 303 K for a 5-hour exposure period. Results show an inversely proportional trend in corrosion rates against raised concentrations of the inhibitor together with an increasing inhibitor efficiency [22]. While there was no inhibition (IE % = 0 %), the corrosion rate was 4.93 $gm^{-2}h^{-1}$ at zero concentration of the inhibitor [23]. Upon introducing 0.1 mM MAPTT, the corrosion rate drastically reduced to 0.82 $gm^{-2}h^{-1}$, with an IE of 40.1 %. Further increases in the inhibitor concentration yielded progressive reductions in C_R, reaching a minimum of 0.33 $gm^{-2}h^{-1}$ at 1 mM MAPTT. This concentration achieved the maximum IE % of 94.3 %. Figure 2 highlights the steep decline in the corrosion rate and a rapid rise in IE % as the MAPTT concentration increases up to 0.5 mM, after which the changes become marginal. At 0.5 mM, the IE stabilizes around 92.7 %, indicating that this concentration is near-optimal.

The enhanced IE % with increasing concentration is attributed to the adsorption of MAPTT onto the steel surface, which forms a protective layer, thereby reducing the metal's direct exposure to the aggressive acidic medium. This adsorption is likely facilitated by the presence of heteroatoms (N, S, and O) and π-electron systems in the MAPTT molecule, which interacts with steel via chemisorption and also physisorption processes. Langmuir adsorption behavior observed suggests that the inhibitor molecules cover the steel surface uniformly, providing a robust barrier against corrosive agents [24, 25]. The marginal improvement in IE % beyond 0.5 mM may result from saturation of the adsorption sites on the metal surface.

3.2. Influence of immersion time

At 303 °K, effect of exposure period and inhibitor concentration on the corrosion rate and IE % of MAPTT for tested metal in 1 M HCl was investigated. The outcomes, illustrated in Figure 3, demonstrate a clear dependence of both C_R and IE % on immersion time and inhibitor dosage. C_R decreases significantly with rising inhibitor dosage for the exposure periods. After 1 h of exposure, the C_R at the lowest inhibitor concentration (0.1 mM) is 0.99 $gm^{-2}h^{-1}$, which is substantially higher than the value at 1 mM MAPTT (0.41 $gm^{-2}h^{-1}$). A similar trend is observed for longer immersion times, C_R progressively decreasing as the inhibitor concentration increases [26]. Interestingly, CR generally stabilizes after 24 hours of immersion for concentrations ≥0.4 mM. For example, at 0.5 mM, C_R remains relatively constant from 24 to 48 hours at ~0.31 $gm^{-2}h^{-1}$. This behavior refers to forming a persistent and protective inhibitory layer on the steel, preventing further corrosion over prolonged exposure [27].

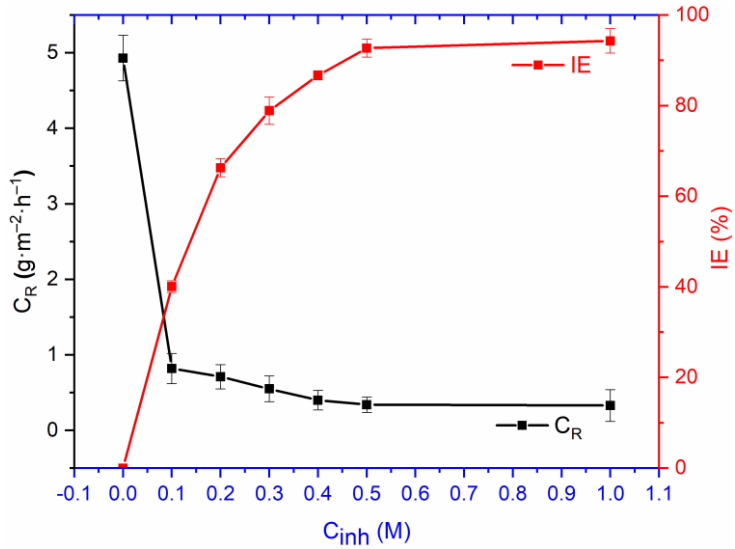

Figure 2: Effect of MAPTT concentration on C_R and IE % in HCl at 303 °K.

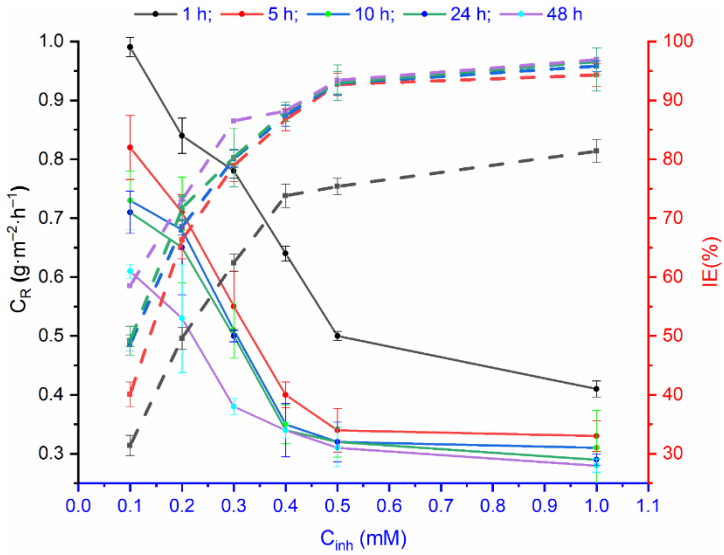

Figure 3: Effect of MAPTT concentration on C_R and IE of steel in 1 M HCl at 303 °K.

IE improves significantly with increasing exposure period, particularly for lower MAPTT concentrations. At 0.1 mM, IE % increases from 31.4 % after 1 hour to 58.5 % after 48 hours. Similarly, at 0.2 mM, IE % rises from 49.6 % after 1 hour to 73.1 % after 48 hours. This trend reflects the gradual adsorption and stabilization of MAPTT molecules on the mild steel surface. For higher inhibitor concentrations (≥0.4 mM), IE % remains consistently high (>87 %) even after prolonged immersion [28]. At 1 mM MAPTT, IE % reaches a maximum of 96.9 % after 48 hours, indicating that saturation of the adsorption sites has been achieved. This high level of IE % highlights the good performance of MAPTT as a inhibitor in acidic environments.

Combined effect of exposure period and inhibitor concentration demonstrates that MAPTT provides excellent corrosion protection at relatively low concentrations. At 0.5 mM MAPTT, IE % is already 92.7 % after 5 hours and increases slightly to 93.4 % after 48 hours. This suggests that MAPTT achieves near-optimal IE % within a short immersion period, with minimal additional improvement over time for higher concentrations. The high IE % of MAPTT can be attributed to its adsorption on the tested metal, forms a protected layer which reduces steel dissolution in HCl [29]. The gradual improvement in IE % with immersion time at lower concentrations may result from the slow but progressive adsorption of MAPTT molecules. Conversely, the consistent and high IE % observed at higher concentrations indicates the rapid saturation of adsorption sites, resulting in robust protection.

3.3. Temperature-dependent corrosion inhibition efficiency

The effect of temperature (313-333 °K) on the IE % of MAPTT was investigated by conducting weight loss measurements for various inhibitor concentrations. The results are postulated in Figure 4. CR decreases clearly with raising MAPTT concentration across all temperatures, demonstrating the IE of MAPTT as a corrosion inhibitor. At the lowest dosage (0.1 mM), C_R reduces from 0.82 gm^{-2}h^{-1} at 303 °K to 0.68 gm^{-2}h^{-1} at 333 °K, indicating a slight improvement in corrosion protection as the temperature rises. In the case of the highest dosage of 1 mM, C_R drops from 0.33 gm^{-2}h^{-1} at 303 °K to 0.28 gm^{-2}h^{-1} at 333 °K. The decrease of C_R with increasing temperature may be attributed to the fact that MAPTT molecules are more adsorbed on mild steel surfaces at elevated temperatures. This gives evidence that the inhibitor forms a stable and strong protective layer under all thermal conditions [30]. IE % is improved not only by inhibitor concentration but also increases with temperature. Thus, at the concentration 0.1 mM, the capturing percentage, IE %, increases from 40.1 % at 303 °K to 47.9 % at 333 °K, and for the concentration at 1 mM, the IE% increases from 94.3 % at 303 °K to 98.1 % at 333 °K. Hence, the increase in IE % with temperature supports the view that MAPTT follows a mixed adsorption mechanism wherein the inhibitor is found both chemisorbed and physiosorbed [31].

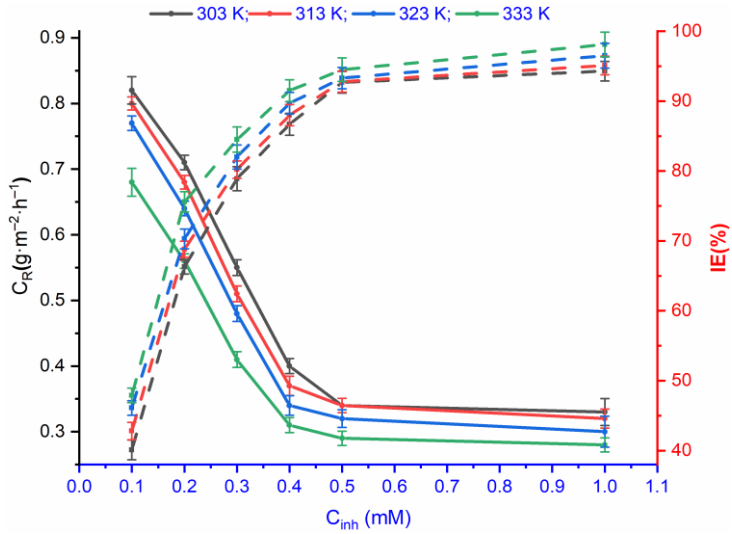

Figure 4: Temperature-dependent C_R and IE% of MAPTT in HCl solution.

All inhibitor concentrations (≥0.5 mM) have been found to attain high IE % (>92 %) for different temperatures tested consistently. Thus, at 0.5 mM, it is 92.7 % at 303 °K and slightly increases to 94.5 % at 333 °K. While at 1 mM, it reaches near-complete protection of 98.1 % at 333 °K. This is a clear reflection of the strength of MAPTT in terms of corrosion resistance at high temperatures.

3.4. Adsorption behavior of MAPTT

Adsorption characteristics of MAPTT on the steel surface were evaluated using the Langmuir isotherm model. The Langmuir model equation is expressed as Eq. 9:

$$\frac{C_{inh}}{\theta} = \frac{1}{K_{ads}} + C_{inh} \quad (9)$$

Where C_{inh} represents the inhibitor dosage, θ denotes the surface coverage (determined by $\theta = \frac{IE}{100}$), K_{ads} is the adsorption equilibrium constant.

The plot of C_{inh}/ θ versus C_{inh} (Figure 5) shows a linear relationship, confirming that the adsorption of MAPTT follows the Langmuir adsorption isotherm. The high linear regression coefficient (R2=0.99008) supports this conclusion [32]. From the intercept of the Langmuir plot ($\frac{1}{K_{ads}} = 0.11582$), the parameter K_{ads} can be calculated as Eq. 10:

$$K_{ads} = \frac{1}{\text{Intercept}} = \frac{1}{0.115821} = 8.63M^{-1} \quad (10)$$

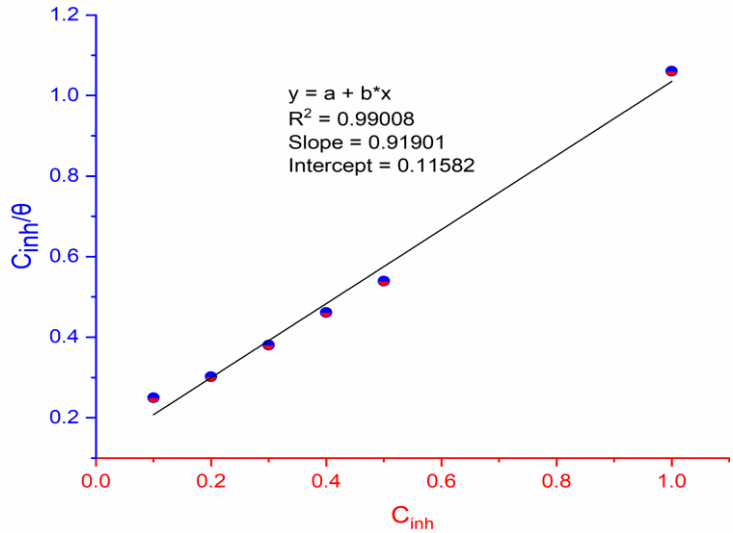

Figure 5: Plot of langmuir adsorption for MAPTT adsorption on metal surface in 1 M HCl.

Standard free energy (ΔG^{o}_{ads}) was determined using the following equation 11:

$$\Delta G^{o}_{ads} = -RT\ln(K_{ads}\times 1000) = -(8.314\times 303)\ln(8.63\times 1000) = -22.83 \text{kJ/mol} \quad (11)$$

Where, R parameter is constant of gas, T is temperature, K_{ads} is multiplied by 1000 to convert to L/mol.

The calculated value of the ΔG_{ads}^{o} for MAPTT was found to be -22.83 $kJmol^{-1}$, indicating a mixed adsorption mechanism involving both physisorption and chemisorption. Generally, Values of ΔG_{ads}^{o} around -20 $kJmol^{-1}$ or less suggest physisorption, which involves weak van der Waals interactions. Value around -40 $kJmol^{-1}$ or more proposed chemical adsorption, which represents the formation of coordination bonds between the inhibitor and the iron d-orbitals. The intermediate ΔG_{ads}^{o} value obtained in this study implies that the adsorption of MAPTT on steel is primarily physisorption, with some contributions from chemisorption [33, 34]. The negative value of ΔG_{ads}^{o} refers to the adsorption process of MAPTT is a spontaneous one. The combination of physisorption and chemisorption mechanisms significantly enhances corrosion resistance by reducing the direct exposure of the metal to the acidic environment.

3.5. DFT and quantum chemical

This is obtained from Figure 6, viewed at the optimized conformational geometry of MAPTT. Such structures are planar and compact and thus are good for specific adsorption to the surface. The following are some of the salient structural features:

- Heteroatoms (N, S, O): These are the active sites for interaction with the steel surface owning to electron pairs of heteroatoms.
- **Aromatic Rings:** The delocalized π-electrons in the aromatic systems enable π–d orbital interactions, improving the strength of adsorption.
- **Thione Group (-C=S):** This group contributes to the strong adsorption through bonding with the Fe d-orbitals.

The overall structure of MAPTT depicts that it can move ahead towards forming a stable and protective film over the mild steel surface against exposure to corrosive agents [35]. The HOMO is localized primarily around the heteroatoms (N and S) and the aromatic rings, thus identifying them as the electron donor centers for this observation:

- **Electron Donation:** The HOMO represents the regions with the highest electron density, which can interact with the Fe d-orbitals on the mild steel surface through chemisorption.
- **Localization on Active Centers:** The significant contribution of heteroatoms (N, S) to the HOMO indicates their role in forming coordination bonds with the metal surface.

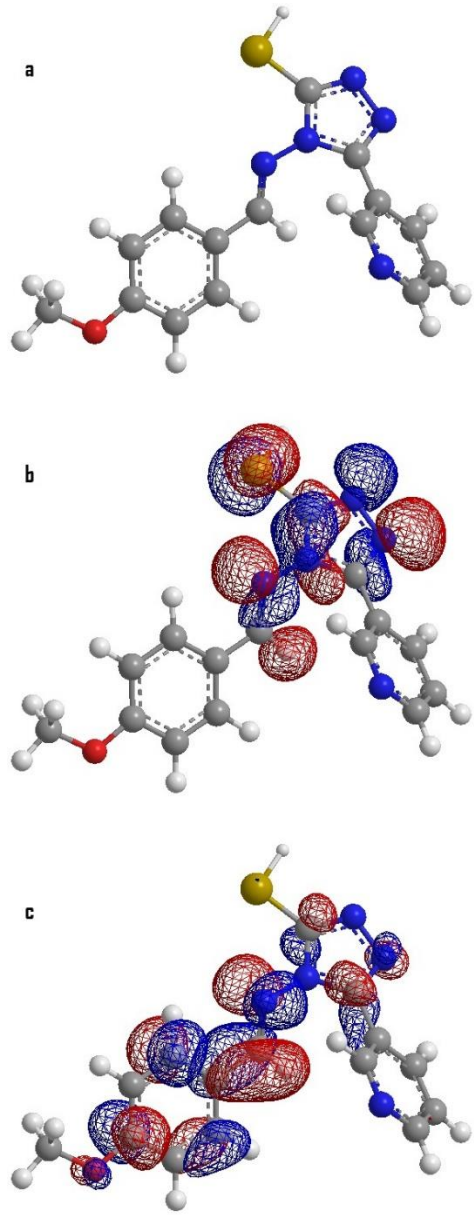

Figure 6: (a) Molecular structure, (b)HOMO, and (c)LUMO distributions of MAPTT highlighting active sites for corrosion inhibition.

With high electron density in these regions, MAPTT acts as a good electron donor for stronger chemisorption and hence better corrosion IE %. The LUMO is spread over the aromatic rings and sulfur-containing groups, suggesting the acceptor of MAPTT from the surface [36]. Points of interest include:

- **Back-Donation Capability:** The LUMO regions allow the MAPTT to accept electrons from tested metal, stabilizing the adsorption through physisorption interactions.
- **Stabilization of Adsorption:** The overlap of LUMO regions with the metal's electron cloud enhances the adsorption strength and contributes to the forming of a robust protected layer.

Complementary nature of HOMO and LUMO interactions enables MAPTT to establish dual adsorption (chemisorption and physisorption) on the surface. The optimized structure of MAPTT, along with the HOMO and LUMO distributions, highlights its ability to interact strongly with surface. The localization of HOMO and LUMO on key functional groups (heteroatoms, aromatic rings) facilitates dual adsorption through electron donation and back-donation mechanisms [37]. These properties, combined with the moderate HOMO-LUMO gap, explain the high IE % of MAPTT in acidic environments.

The quantum chemical parameters of MAPTT (Table 1), including I, A, ΔE, η, χ, and ΔN, were calculated to assess its performance for steel in HCl. These parameters provide insights into the electronic properties and adsorption behavior of MAPTT on the mild steel surface. The high absolute value of E_{HOMO} (-8.035 eV) indicates the inhibitor's low tendency to donate electrons. However, MAPTT's ability to donate electrons to unoccupied d-orbitals of surface of metal enhances its interaction through chemisorption. The moderate E_{LUMO} (-2.437 eV) reflects the inhibitor's ability to accept electrons from the metal surface, contributing to back-donation interactions and physisorption. A moderate ΔE (5.598 eV) suggests a balance between chemical stability and reactivity. Lower energy gaps are often associated with higher IE % due to stronger adsorption on the metal surface. The moderate hardness (η=2.799 eV) indicates MAPTT's ability to resist deformation in its electronic structure, promoting stability during adsorption on the metal surface. The electronegativity value (χ=5.236 eV) shows that MAPTT has a strong tendency to attract electrons, enhancing its adsorption through physical interactions. The negative value of ΔN (-0.131) implies that MAPTT donates electrons to the metal surface, promoting chemisorption. This is consistent with the mixed adsorption mechanism observed experimentally. The calculated parameters reveal that MAPTT exhibits a mixed adsorption mechanism involving both chemisorption and physisorption. The donation of electrons from MAPTT to the metal surface strengthens the protective adsorption layer, while the ability to accept electrons further stabilizes this interaction. The moderate ΔE and η support its reactivity and stability, ensuring efficient corrosion inhibition. These quantum chemical findings align well with the experimental results, where MAPTT demonstrated high IE %.

Table 1: Predation parameters of MAPTT and their implications for corrosion.

Parameter	Value (eV)
HOMO	8.035
LUMO	2.437
I	8.035
A	2.437
ΔE	5.598
η	2.799
χ	5.236
ΔN	-0.131

A moderate HOMO-LUMO energy gap (ΔE = 5.598 eV) in MAPTT suggests a favorable balance between chemical stability and reactivity, which is crucial for efficient inhibition. A smaller ΔE facilitates efficient charge transfer between MAPTT and the surface, enhancing adsorption processes. This characteristic is essential for applications requiring long-term protection of metal components, such as in oil refineries, marine industries, and chemical processing plants [38]. The concept of electronegativity is pivotal in understanding the interactions of MAPTT and the surface [39]. Furthermore, the fraction of electrons transferred (ΔN) provides insight into the electron-donating capability of the inhibitor. A negative ΔN value signifies that MAPTT acts as an electron donor, transferring charge to the mild steel surface. This electron donation facilitates chemisorption, enhancing the strength and stability of the adsorption layer formed on the metal. Such strong interactions are beneficial for corrosion protection. However, while this suggests good laboratory

performance, potential industrial limitations may include long-term stability under variable field conditions and cost implications for large-scale synthesis and application, which merit further investigation in future studies. This interaction involves both physisorption and chemisorption mechanisms, ensuring durability and high IE %, even at elevated temperatures. Such properties make MAPTT suitable for high-temperature industrial processes like acid pickling and metal cleaning. Economically, MAPTT's high IE% at low concentrations (e.g., 92.7 % at 0.5 mM) reduces the required inhibitor dosage, leading to cost-effectiveness in large-scale applications. Additionally, the environmental sustainability of MAPTT, due to the absence of toxic heavy metals, aligns with the growing demand for eco-friendly corrosion inhibitors in green manufacturing and sustainable engineering solutions.

3.6. Surface morphology analysis by SEM

To further validate the corrosion inhibition performance of MAPTT on mild steel in 1 M HCl, Scanning Electron Microscopy (SEM) analysis was conducted. Figure 7 displays the SEM micrographs of the mild steel surface after immersion for 5 hours under two different conditions:

- (a) in 1 M HCl without MAPTT, and
- (b) in 1 M HCl containing 1.0 mM MAPTT.

In Figure 7a, representing the uninhibited sample, the surface appears severely damaged and rough, characterized by pitting, grooves, and surface inhomogeneities. This clearly indicates the aggressive attack of the acidic medium on the mild steel surface, leading to significant material degradation due to uniform and localized corrosion.

In contrast, Figure 7b shows the SEM image of the steel specimen immersed in the same corrosive medium but with the addition of 1.0 mM MAPTT. The surface is noticeably smoother, more uniform, and relatively free from deep corrosion pits or etching marks, suggesting the effective adsorption of MAPTT molecules onto the steel surface. This protective film hinders direct contact between the metal and the corrosive environment, significantly reducing corrosion activity.

The observable differences between the two micrographs confirm the formation of a protective barrier by MAPTT, which acts to retard the corrosion process. These morphological results are consistent with the findings from weight loss measurements and thermodynamic studies, reinforcing the role of MAPTT as a potent corrosion inhibitor that provides surface passivation through both physical and chemical adsorption mechanisms.

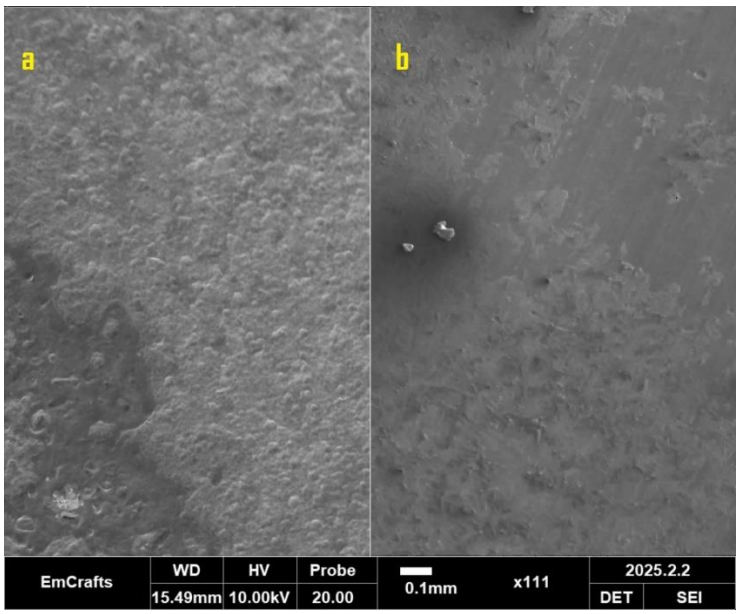

Figure 7: SEM micrographs of mild steel surface after 5 hours immersion in 1 M HCl (a) without MAPTT inhibitor, showing severe corrosion damage, and (b) with 1.0 mM MAPTT, showing a smoother and protected surface due to inhibitor adsorption.

3.7. Suggested mechanism

The presence of heteroatoms such as nitrogen, sulfur, and oxygen in the MAPTT molecule facilitates strong adsorption onto the steel surface, enhancing its protective capability. These atoms possess electrons pairs, which can interacts with the d-orbitas of Fe atoms, forming strong coordination bonds (chemisorption). Additionally, the π-electrons in the aromatic rings of MAPTT contribute to interactions with the metal surface, enhancing adsorption. Besides that, the capacity of the MAPTT to accept electrons from mild steel plays a role in the adsorption characteristics through back-donation, by allowing the consequent stabilization of the layer formed as the result of adsorption [40]. A very firm and robust barrier protection fortified by acidic corrosive act is thus provided. Once adsorbed, MAPTT forms a hydrophobic protected layer that isolates the steel surface from HCl medium. The formation of this layer, therefore, inhibits and minimizes access of competing H^+ ions as well as other aggressive species to the protecting layer and, in turn, minimizes the rate of dissolution of metal and subsequent corrosion. Experimental findings reveal that there is only a slight change in IE % at different temperature levels for MAPTT, which indicates that in higher temperatures, chemisorption dominates. The energy of the thermal environment enhances the force of MAPTT and the metal surface, thus rendering it stronger adsorbed. Theoretical calculations show that MAPTT has a moderate ΔE with irrespective HOMO-LUMO energy gaps alongside high χ. Therefore, these two features favor MAPTT to victimize the mild steel surface. ΔN reveals that MAPTT donates electrons to the metal, thereby supporting chemisorption which agrees with the proposed dual adsorption mechanism.

The mechanism of inhibition for corrosion by MAPTT can be summed up as follows:

1. Adsorption of MAPTT on the surface through heteroatoms and π-electrons.
2. Formation of a compact, hydrophobic protective layer, reducing the interaction of metallic surface with the HCl medium.
3. Combined physisorption and chemisorption processes stabilize the adsorption layer.
4. Enhanced protection at elevated temperatures due to stronger chemisorption interactions.

3.8. Comparison of IE % with similar inhibitors

The inhibition efficiency (IE%) of MAPTT was critically compared with other reported organic inhibitors containing heteroatoms (N, S, O) and aromatic systems-common structural features that are known to enhance adsorption onto metal surfaces. As presented in Table 2, this comparison highlights MAPTT's superior inhibition performance, which can be attributed to its unique structural configuration and favorable electronic properties. MAPTT achieved a maximum IE % of 94.3 % at 303 K and 98.1 % at 333 K at a relatively low concentration of 1.0 mM, demonstrating not only high effectiveness at ambient conditions but also remarkable thermal stability. When compared to structurally related compounds:

- 2-Chloro-3-formyl quinoline and Thiadiazole Schiff base (HL) exhibit moderate efficiencies (~83–88 %) at similar concentrations.

Table 2: Comparative inhibition efficiencies of various organic molecules in 1 M HCl.

Inhibitor	Maximum IE %	Concentration (mM)	Medium	Reference
MAPTT	94.3 % (303 °K)	1.0	1 M HCl	This work
2-Chloro-3-formyl quinoline	88.2 %	≈ 1.0	1 M HCl	[41]
Thiadiazole Schiff base (HL)	83.9 %	1.0	1 M HCl	[42]
1-Octyl-3-methylimidazolium hydrogen sulfate	92.0 %	5.0	1 M HCl	[43]
1-Octyl-3-methylimidazolium chloride	92.0 %	5.0	1 M HCl	[43]
1-Butyl-3-methylimidazolium hydrogen sulfate	80.0 %	5.0	1 M HCl	[43]
HMAP	90.8 %	≈ 2.4	1 M HCl	[44]
CSB-1	97.3 %	≈ 1.0	1 M HCl	[45]
5-Thiol-1,2,4-triazole-3-amine	90.0 %	1.0	1 M HCl	[46]

- Ionic liquid-based inhibitors such as 1-octyl-3-methylimidazolium derivatives reach up to 92 %, but only at higher concentrations (5.0 mM), which raises concerns regarding economic and environmental impact.
- HMAP and 5-thiol-1,2,4-triazole-3-amine both offer reasonable efficiencies around 90 %, but still fall short of MAPTT, especially under elevated temperature conditions.
- Only CSB-1, at 97.3 %, shows slightly higher efficiency—but at a comparable concentration and without explicit temperature-dependent performance data.

The enhanced corrosion inhibition performance of MAPTT can be directly correlated to the following molecular-level features:

1. Presence of Multiple Heteroatoms (N, S, O): These atoms provide lone electron pairs that coordinate effectively with the d-orbitals of Fe atoms on the steel surface, strengthening adsorption and promoting chemisorption.
2. Extended Conjugation and π-Systems: The inclusion of pyridine, triazole, and benzylidene groups facilitates strong π–d interactions, reinforcing the adsorption film's integrity.
3. Moderate HOMO–LUMO Energy Gap (ΔE = 5.598 eV): This optimal gap indicates a balance between molecular reactivity and stability, enhancing MAPTT's ability to both donate and accept electrons during adsorption, a key factor in dual adsorption behavior.
4. Dual Adsorption Mechanism (Physisorption + Chemisorption): Langmuir adsorption isotherm analysis, along with thermodynamic evaluation (ΔG_{ads}^{o}=-22.83 KJ/mol), confirms a mixed adsorption mode, providing enhanced film stability under varying operational conditions.

In contrast to many conventional inhibitors that lose efficiency at elevated temperatures due to desorption, MAPTT retains and even improves its inhibition performance at 333 °K. This is a critical advantage for real-world applications, such as acid pickling, industrial cleaning, petrochemical processing, and desalination systems, where high-temperature acid exposure is common. Furthermore, MAPTT achieves high IE % at low concentrations, making it cost-effective and environmentally favorable. Its molecular versatility, strong interaction with the metal surface, and temperature resilience make it a robust candidate for large-scale industrial applications. Notably, MAPTT's performance exceeds that of most inhibitors in its class under similar test conditions, positioning it as a leading corrosion inhibitor among triazole-based compounds. In summary, the comparison in Table 2 demonstrates that MAPTT not only rivals but surpasses many structurally analogous inhibitors in both efficiency and practical applicability. Its unique chemical structure, supported by both experimental data and DFT calculations, underscores its potential as a next-generation inhibitor for protecting mild steel in highly corrosive environments.

4. Conclusion

This study confirms the effectiveness of MAPTT as a corrosion inhibitor for mild steel in 1 M HCl, supported by both experimental and theoretical analyses. The key findings are summarized as follows:

1. MAPTT achieved a maximum inhibition efficiency (IE %) of 94.3 % at 303 °K and 98.1 % at 333 °K at an optimal concentration of 1.0 mM. The increase in IE % with rising concentration and temperature confirms the strong inhibitory performance of MAPTT in acidic environments.
2. The adsorption of MAPTT onto the mild steel surface followed the Langmuir isotherm, indicating monolayer coverage. Thermodynamic analysis revealed a mixed adsorption mechanism, involving both physisorption and chemisorption, with a calculated free energy of adsorption $\Delta G_{ads}0$ ($-22.83\ kJ.mol^{-1}$).
3. Unlike many conventional inhibitors, MAPTT retained its performance even at elevated temperatures, where chemisorption became more dominant. This thermal stability makes MAPTT a promising candidate for industrial applications such as acid cleaning, descaling, and metal pickling processes.
4. Quantum chemical analyses supported the experimental results, with a moderate HOMO–LUMO energy gap (ΔE=5.598 eV) and a negative electron transfer fraction (ΔN=−0.131), indicating strong interaction with the steel surface via electron donation and back-donation.
5. MAPTT outperformed several structurally related inhibitors, particularly at higher temperatures, due to its optimized molecular structure and dual adsorption behavior.
6. The inhibitor demonstrated high IE% at relatively

low concentrations, emphasizing its cost-effectiveness and environmental compatibility, which are essential criteria for industrial corrosion management.

7. Surface morphology analysis using SEM confirmed the protective role of MAPTT, revealing a smoother and less damaged steel surface in the presence of the inhibitor, which supports the formation of an adsorbed barrier layer that effectively reduces corrosion.
8. Limitation: This study was limited to weight loss measurements. Although the results are promising, the absence of electrochemical techniques such as Potentiodynamic Polarization (PDP) and Electrochemical Impedance Spectroscopy (EIS) is acknowledged. These techniques will be incorporated in future work to further validate the inhibition mechanism and kinetics of MAPTT.

5. References

1. Wang R, Lin S, Song W, Liu Z. Occurrence and potential endocrine benzotriazoles disrupting effects of and thiazolinones in municipal wastewater treatment plants. Chemosphere. 2014; 112:288-294. https://doi.org/10.1016/j.chemosphere. 2014.04.007.
2. Khaled KF, Hackerman N. Synergistic inhibition of aluminum alloy corrosion by mixtures of 2mercapto-benzothiazole and potassium iodide. J Electrochem Soc. 2003;150(2). https://doi.org/10. 1149/1.1539013.
3. Quraishi MA, Ebenso EE. Synergistic effect of ammonium nitrate and iodide ions on the corrosion inhibition of mild steel in acidic medium by some 1,3,4-oxadiazoles. Corr Sci. 2014; 85:25-35. https://doi.org/10.1016/j.corsci.2014.03.022.
4. Vaszilcsin N, Ordodi V, Borza A. Corrosion inhibitors from expired drugs. Inter J Pharm. 2012; 431(1-2): 2414. https://doi.org/10.1016/j.ijpharm. 2012. 04.015.
5. Al-Shafey HI, Hameed RA, Ali FA, Aboul-Magd AE, Salah M. Effect of expired drugs as corrosion inhibitors for carbon steel in 1M HCL solution. Int J Pharm Sci Rev Res. 2014; 27(1):146-52. https://doi.org/10.15344/2394-8376/2024/146.
6. Dehghani A, Ghahremani P, Mostafatabar AH, Ramezanzadeh B. Plant extracts: Probable alternatives for traditional inhibitors for controlling alloys corrosion against acidic media-A review. Biomass Con Bioref. 2024; 14(6):7467-86. https://doi.org/10. 1007/s13399-023-03907-0.
7. Gong W, Yin X, Liu Y, Chen Y, Yang W. 2-Amino4-(4-methoxyphenyl)-thiazole as a novel corrosion inhibitor for mild steel in acidic medium. Prog Org Coat. 2019; 126:150-161. https://doi.org/10.1016/j.porgcoat.2018.10.001.
8. Dehghani A, Berdimurodov E, Verma C, Verma DK, Berdimuradov K, Quraishi MA, Aliev N. Constructing efficacy: A novel perspective on organic corrosion inhibitors and interfacial interactions. Chem Papers. 2024; 78(3):1367-97. https://doi.org/10.1007/s11696023-02586-4.
9. Döner A, Solmaz R, Özcan M, Kardaş G. Experimental and theoretical studies of thiazoles as corrosion inhibitors for mild steel in sulphuric acid solution. Corr Sci. 2011; 53(9):2902-2913. https://doi.org/10.1016/j.corsci.2011.05.034.
10. Yang X, Li F, Zhang W. 4-(Pyridin-4-yl) thiazol-2amine as an efficient non-toxic inhibitor for mild steel in hydrochloric acid solutions. RSC Adv. 2019;9 (19):10454-64. https://doi.org/10.1039/C9RA00672H.
11. Abdulwali N, Mohammed F, Al Subari A, Ghaddar H, Guenbour A, Bellaouchou A, Essassi EM, Cottis RA. Effect of thiazole derivatives on the corrosion of mild steel in 1 M HCl solution. Intern J Electrochem Sci. 2014; 9(11):6402-15. https://doi.org/10.20964/2014. 11.20.
12. Zunita M, Rahmi VA. Advancement of plant extract/ionic liquid-based green corrosion inhibitor. Chem Africa. 2024; 7(2):505-38. https://doi.org/10.1007/s42250-023-00426-0.
13. Abuelela, A.M., Bedair, M.A., Gad, E.S. et al. Exploring the synthesis, characterization, and corrosion inhibition of new tris-thiosemicarbazone derivatives for acidic steel settings using computational and experimental studies. Sci Rep. 2024,14, 13310. https://doi.org/10.1038/s41598-024-64199-x.
14. Gad, E.S., Abbas, M.A., Bedair, M.A. et al. Synthesis and applications of novel Schiff base derivatives as corrosion inhibitors and additives for improvement of reinforced concrete. Sci Rep. 2023; 13:15091. https://doi.org/10.1038/s41598-023-41165-7
15. Akpan ED, Singh AK, Lgaz H, Quadri TW, Shukla SK, Mangla B, Dwivedi A, Dagdag O, Inyang EE, Ebenso EE. Coordination compounds as corrosion inhibitors of metals: A review. Coord Chem Rev. 2024; 499:215503. https://doi.org/10.1016/j.ccr. 2024. 215503.
16. Toghan A, Alduaij OK, Fawzy A, Mostafa AM, Eldesoky AM, Farag AA. Effect of adsorption and interactions of new triazole-thione-schiff bases on the corrosion rate of carbon steel in 1 M HCl solution: theoretical and experimental evaluation. ACS Omega. 2024;9(6):6761-6772. https://doi.org/10.1021/acsomega.3c08127.
17. Mortadi K, El Amri A, Ouakki M, Hsissou R, Jebli A, Lebkiri A, Safi Z, Wazzan N, Berisha A, Cherkaoui M, Hbaiz EM. Electrochemical and theoretical studies on a bioactive Juniperus oxycedrus essential oil as a potential and ecofriendly corrosion inhibitor for mild steel in 1.0 M HCl environment.

Inorg Chem Commun. 2024; 112196. https://doi.org/10.1016/j.inoche.2024.112196.
18. ASTM International, Standard Practice for Preparing, Cleaning, and Evaluating Corrosion Test, 2011, 1-9.
19. NACE International, Laboratory Corrosion Testing of Metals in Static Chemical Cleaning Solutions at Temperatures below 93 °C (200 °F), TM0193-2016-SG, 2000.
20. Frisch MJ, Trucks GW, Schlegel HB, Scuseria GE, Robb MA, Cheeseman JR, et al. Gaussian 03, Revision B. 05, Gaussian, Inc., Wallingford, CT, 2004.
21. Koopmans T. Über die Zuordnung von Wellenfunktionen und Eigenwerten zu den einzelnen Elektronen eines Atoms. Physica. 1934; 1(1-6):10413. https://doi.org/10.1016/S0031-8914(34)90011-2.
22. Lavanya M, Ghosal J, Rao P. A comprehensive review of corrosion inhibition of aluminium alloys by green inhibitors. Canadian Metallur Quart. 2024; 63(1):119-29. https://doi.org/10.1080/00084433.2024.1132326.
23. Bhatia AK, Dewangan S. N-heterocyclics as corrosion inhibitors: miscellaneous. In Handbook of Heterocyclic Corrosion Inhibitors 2024 (pp. 249-270). CRC Press. https://doi.org/10.1201/9781003331285.
24. Touir R, Errahmany N, Rbaa M, Benhiba F, Doubi M, Kafssaoui EE, Lakhrissi B. Experimental and computational chemistry investigation of the molecular structures of new synthetic quinazolinone derivatives as acid corrosion inhibitors for mild steel. J Mol Struct. 2024; 1303:137499. https://doi.org/10.1016/j.molstruc.2024.137499.
25. Abd El Wanees S, Kamel MM, Ibrahim M, Rashwan SM, Atef Y, Abd Elsadek MG. Corrosion inhibition and synergistic effect of ionic liquids and iodide ions on the corrosion of C-steel in formation water associated with crude oil. J Umm Al-Qura University Appl Sci. 2024; 10(1):107-19.
26. Sehrawat R, Vashishth P, Bairagi H, Shukla SK, Kumar H, Ji G, Mangla B. Coordination bonding and corrosion inhibition characteristics of chalcone compounds for metals: An inclusive review based on experimental as well as theoretical perspectives. Coordin Chem Rev. 2024; 514:215820. https://doi.org/10.1016/j.ccr.2024.215820.
27. González-Parra JR, Di Turo F. The Use of Plant extracts as sustainable corrosion inhibitors for cultural heritage alloys: a mini-review. Sustainability. 2024; 16(5):1868. https://doi.org/10.3390/su16051868.
28. Zhao Y, Teng X, Xu Z. The scale inhibition mechanism of sodium humate on heat transfer surface: Insights from electrochemical experiments, quantum chemical calculations, and molecular dynamics simulation. Inter J Heat Mass Transfer. 2024;220: 124966. https://doi.org/10.1016/j.ijheatmasstransfer.2023.124966.
29. Namdar-Asl H, Fakheri F, Pour-Ali S, Tavangar R, Hejazi S. Synthesis and corrosion inhibition study of 1aminobenzotriazole for mild steel in HCl solution: electrochemical, surface analysis, and theoretical investigations. Prog Color Colorant Coat. 2024; 17(1): 61-74. https://doi.org/10.30502/PCCC.2023.359903.
30. Touir R, Errahmany N, Rbaa M, Benhiba F, Doubi M, Kafssaoui EE, Lakhrissi B. Experimental and computational chemistry investigation of the molecular structures of new synthetic quinazolinone derivatives as acid corrosion inhibitors for mild steel. J Mol Struct. 2024; 1303:137499. https://doi.org/10.1016/j.molstruc.2023.137499.
31. Coy-Barrera CA, Quiroga D. In silico evaluation for the design of coumarin-type compounds based on phenol and naphthol rings as a coating in carbon steel corrosion processes: DFT B3LYP calculations, synthesis and electrochemical characterization. Prog Org Coat. 2024; 188:108266. https://doi.org/10.1016/jporgcoat.2023.108266.
32. Sheit HM, Mohan KS, Gunavathy KV, Mohamed MV, Subhapriya P, Samsathbegum A, Sindhuja GH. Investigation on the corrosion inhibition efficiency of 2,4-diphenyl-3-aza bicyclo [3.3.1] nonan-9-one in carbon steel immersed in acidic media. Chem Phys Impact. 2024; 8:100521. https://doi.org/10.1016/j.chphi.2023.100521.
33. Anadebe VC, Chukwuike VI, Nayak KC, Ebenso EE, Barik RC. Combined electrochemical, atomic scaleDFT and MD simulation of Nickel based metal organic framework (Ni-MOF) as corrosion inhibitor for X65 pipeline steel in CO_2-saturated brine. Mater Chem Phys. 2024; 312:128606. https://doi.org/10.1016/j.matchemphys.2023.128606.
34. Laarioui A, Chaouki I, Hmada A, El Magri A, Errahmany N, El Hajri F, Dkhireche N, Bakkali S, Touir R, Boukhris S. Corrosion inhibition effect of the synthetized chromen-6-one derivatives on mild steel in 1.0 M HCl electrolyte: electrochemical, spectroscopic and theoretical studies. Mor J Chem. 2024; 12(2):570-93. https://doi.org/10.48317/IMIST.PRSM/morjchem-v12i2.40860.
35. Pai GD, Rathod MR, Rajappa SK, Kittur AA. Effect of tabebuia heterophylla plant leaves extract on corrosion protection of low carbon steel in 1M HCl medium: Electrochemical, quantum chemical and surface characterization studies. Results Surf Inter. 2024; 15:100203. https://doi.org/10.1016/j.rsurfin.2023. 100203.
36. Dahmani K, Galai M, Rbaa M, Ech-Chebab A, Errahmany N, Guo L, AlObaid AA, Hmada A, Warad I, Touhami ME, Cherkaoui M. Evaluating the efficacy of synthesized quinoline derivatives as corrosion inhibitors for mild steel in acidic environments: An analysis using electrochemical, computational, and surface techniques. J Mol Struct. 2024; 1295:136514. https://doi.org/10.1016/j.molstruc.2023.136514.
37. Akrom M, Rustad S, Dipojono HK. A machine learning approach to predict the efficiency of corrosion inhibition by natural product-based organic inhibitors. Phys Scripta. 2024; 99(3):036006. https://doi.org/10.1088/1402-4896/ace0d2.

38. Fang J, Li J. Quantum chemistry study on the relationship between molecular structure and corrosion inhibition efficiency of amides. J Mol Struct. 2002; 593(1-3):179-85. https://doi.org/10.1016/ S0166-1280(02)00316-0
39. Lukovits I, Kalman E, Zucchi F. Corrosion inhibitors-correlation between electronic structure and efficiency. Corrosion. 2001; 57(1):3-8. https://doi.org/10.5006/1.3290328.
40. Fernandes CM, Coutinho MS, Leite MC, Martins V, Batista MP, Faro LV, Al-Rashdi AA, Silva JC, Batalha PN, Lgaz H, Ponzio EA. Green-synthetized βamino-α-carbethoxy ethyl acrylates as corrosion inhibitors for mild steel in acid media: Experimental performance evaluation and atomic/molecular-level modeling. Inorg Chem Commun. 2024; 159:111722. https://doi.org/10.1016/j.inoche.2023.111722.
41. Essien KE, Okon EJ, Archibong IN, Okon OE, George IE. Experimental, quantum chemical and IR spectroscopy studies on the corrosion inhibition of mild steel by 3,5-dimethyl-4-nitroisoxazole in HCl solutions. J Mater Environ Sci. 2024; 15(1):136. https://doi.org/10.26872/jmes.2021.12.6.40.
42. Benachour N, Delimi A, Allal H, Boublia A, Sedik A, Ferkous H, Djedouani A, Brioua S, Boulechfar C, Benzouid H, Houssou A. 3,4-Dimethoxy phenyl thiosemicarbazone as an effective corrosion inhibitor of copper acidic experimental, solution: characterization comprehensive and theoretical investigations. RSC Adv. 2024; 14(18):12533-55. https://doi.org/10.1039/D3RA06847G.
43. Kumar D, K VM, Jain V, Rai B. Accelerating corrosion inhibitor discovery through computational routes: a case of naphthalene 1-thiocarboxamide. Mater Degrad. 2024;8(1):5. https://doi.org/10.1038/s41529-023-00310-7.
44. Narang R, Vashishth P, Bairagi H, Sehrawat R, Shukla SK, Mangla B. Experimental and quantum chemical investigation of corrosion inhibitive action of sertraline on mild steel in acidic medium. Chem Africa. 2024; 24:1-7. https://doi.org/10.1007/s42250-02300437-1.
45. Fang Q, Yang X, Pan G, Yang X, Qi Y. Experimental and density functional theory study of inhibitors on cobalt corrosion for chemical mechanical planarization process. ECS J Solid State Sci Technol. 2024; 13(4): 044007. https://doi.org/10.1149/2162-8777/ acdbe0.
46. Errahmany N, Rouifi Z, Kharbouch O, Tazouti A, Chahboune M, Rbaa M, Larhzil H, Touir R. Molecular structure of synthetized hydrazinylidene based quinoxaline derivatives effect on mild steel corrosion inhibition in 1.0 HCl electrolyte: Synthesis, electrochemical and computational studies. J Mol Struct. 2024; 1308:138146. https://doi.org/10.1016/j.molstruc.2023.138146.
47. Ferkous H, Sedik A, Delimi A, Redjemia R, Abdesalem K, Boulechfar C, Abdennouri A, Madaci A, Berredjem M, Boublia A, Ali MS. A comparative study of novel synthesized sulfamide compounds: Electrochemical, morphological, XPS, and theoretical investigations on copper corrosion inhibition in 1.0 M HCl. J Mol Liq. 2024; 394:123781. https://doi.org/10.1016/j.molliq.2023.123781.
48. Mortadi K, El Amri A, Ouakki M, Hsissou R, Jebli A, Lebkiri A, Safi Z, Wazzan N, Berisha A, Cherkaoui M, Hbaiz EM. Electrochemical and theoretical studies on a bioactive Juniperus oxycedrus essential oil as a potential and ecofriendly corrosion inhibitor for mild steel in 1.0 M HCl environment. Inorg Chem Commun. 2024: 112196. https://doi.org/10.1016/j.inoche.2023.112196.

How to cite this article:
Al-Ali NA, Alamiery A. Corrosion Protection of Mild Steel in Acidic Media by a Triazole-Based Inhibitor: Mechanistic Insights and Performance Evaluation. Prog Color Colorants Coat. 2026;19(1):9-22. https://doi.org/ 10.30509/pccc.2025.167535.1392.